Replacement of R134a with low-GWP fluids in a kW-size reciprocating piston expander: Performance prediction and design optimization

# Replacement of R134a with low-GWP fluids in a kW-size reciprocating piston expander: performance prediction and design optimization

M. Bianchi, L. Branchini*, A. De Pascale, F. Melino, S. Ottaviano, A. Peretto, N. Torricelli

Department of Industrial Engineering
Alma Mater Studiorum – University of Bologna, Italy
e–mail: lisa.branchini2@unibo.it

* Corresponding Author

## ABSTRACT

In this study, low-GWP fluids (R1234yf and R1234ze(E)) have been compared with R134a when used in a kW-size reciprocating piston expander. Semi-empirical models of the pump and the expander are employed to analyze how the different fluids thermodynamic characteristics could influence machines behaviour into real operation of a micro-ORC. Parameters related to thermo-fluid-dynamic fluids properties are updated compared to the original values calibrated over R134a. Results show that the use of HFOs alternative fluids leads to a loss of electric power and expander efficiency, whose detriment depends on fluids properties and on operation strategy. At a given pressure ratio the decrease of power output is close to 21 % and 42 %, while the loss on expander efficiency is more limited, being around 6 % and 11 %, for R1234yf and for R1234ze(E), respectively. Main factors of influence such as saturation pressure, viscosity, heat transfer coefficients and vapor density are discussed. The expander model has also been used to perform the optimization of the built-in volume ratio for each fluid, revealing that a significant enhancement of the expander overall performance could be obtained modifying the intake valve timing, thus reducing under-expansion losses and improving its volumetric efficiency.

**Keywords:** micro-ORC, piston expander, low-GWP fluids, gear pump, performance optimization, semi-empirical model, performance prediction

## INTRODUCTION

Organic Rankine Cycle (ORC) energy systems are considered an efficient solution for low temperature and small size heat recovery applications [1]. The possibility of employment of these systems in micro-scale CHP (Combined Heat and Power) plants for the residential sector has a great potential in a world where the energy saving has become of primary importance. ORCs main strengths are their simplicity and their capacity to retrofit existing thermal system [2]. The European market uptake is still at an early stage, depending on technological issues, such as the selection and design of the system components [3], but also on the structure itself of the electricity generation network, which is mostly of centralized type. The working efficiency of low temperature micro-ORC is still relatively low, due to the small temperature difference between hot source and cold sink resulting in scarce Carnot efficiency, as well as to the lack of appropriate expander machines in the commercial market [4]. In particular, experimental data trends related to existing micro-ORC prototypes (mainly based on volumetric expanders), suggest that design aspects, such as the expander built-in volume ratio, should be still optimized. Indeed, most of the conducted experiments present a mismatch between the cycle expansion ratio and expander expansion ratio, leading to significant over- and/or under-expansion losses. These sources of losses are accountable for a significant drop of the expander isentropic efficiency at maximum power output, resulting in a reduction of the overall cycle efficiency [4].

The referred literature about ORC is abundant and it deals with all the aspects of design, optimization and operation strategy of ORC plants. Among the key factors for ORC design optimization, the selection of the working fluid has been a most discussed topic, since each application can require a different medium and new substances and mixtures have been produced recently for complying with environmental requirements [5].

This topic – being not very essential in high temperature systems – is quite central in low temperature ORCs, where high GWP refrigerants are still adopted as working fluid due to their thermal compatibility with low-grade heat sources. According to the EU F-Gas Regulation 517/2014, in upcoming years the refrigerants with GWP higher than 150 should not be used in new products [6]. The regulation refers to all the utilities adopting greenhouse gases as working fluids (including refrigerators, ORC, heat pumps, etc.) Main examples are the hydrofluorocarbons (HFC) R245fa and R134a, suitable for heat source temperature below 160 °C and 100 °C and characterized by a GWP value equal to 1030 and 1430, respectively [7]. One of the challenges for the researchers in this field has been to identify right replacements for HFCs, which comply with low GWP and, at the same time, reproduce similar thermal performance.

The hydrofluoroolefins (HFOs) are considered good candidates for low temperature application, having very low GWP and similar thermodynamic properties to HFCs. The research about new fluids, in most cases, focuses on how they perform in refrigeration cycles, and on the modifications that has to be done on the hardware for retrofitting existing cooling systems [8]. Indeed, the olefins have been already introduced in some car air-conditioning systems and are commercially available for use in centrifugal chillers, however they still need to be extensively tested into ORC applications. Detailed analyses on olefins performance in ORC systems, both numerical and experimental, mostly refer to the replacement of R245fa in application with heat source temperature between 120 °C and 200 °C.

To mention just a few examples, Eyerer et al. [9] and Yang et al. [10] recently performed experimental analyses to evaluate modern HFO fluids substitutes of R245fa in ORC systems, testing also the materials compatibility [9]. Authors agree that both R1224yd(Z) and R1233zd(E) are suitable for the drop-in replacement of R245fa, since they present thermal efficiency similar to the one obtained with R245fa. However R1233zd(E) presents compatibility issues with the tested materials [9]. They observed instead lower performance for the fluid R1336mzz(E) [10].

On the contrary, studies investigating R134a replacements are still scarce and mainly numerical. For instance, Moles et al. [11] made a theoretical comparison of R1234yf and R1234ze as alternatives to R134a, finding that R1234ze could achieve higher values of net cycle efficiency (around 13.8 %), while R1234yf shows lower performance. They related both results mainly to the difference in pump consumption of the new fluids with respect to R134a. A thermodynamic model was used by Yamada et al. [12] to compare the thermal efficiency of R1234yf and R134a in five different cycle configurations (trilateral, saturated, superheated, sub-critical and super-critical), concluding that the R1234yf can satisfactorily replace R134a in low grade ORC applications. Le et al. [13] presented an efficiency optimization of supercritical ORCs with heat source temperature of 150 °C, comparing several low-GWP fluids in simple and regenerative configuration. Their results showed that the best working fluid may change depending on cycle configuration and on the optimization objective. R1234ze resulted the best solution to optimize the efficiency, while considering the environmental issues.

Literature analyses provide useful thermodynamic evaluation, demonstrating the theoretical potential of new HFOs fluids. However, these studies usually adopt simplified hypothesis such as constant expander and pump efficiency and adiabatic expansion process [11], [12], [13]. This approach risks to overlook the influence of the employed fluid on performance of the component. Indeed, actual operating conditions of the expander and the pump can strongly depend on fluid properties such as density and viscosity, especially if considering volumetric type machines [14]. Fluid conductive coefficient is also an important factor of influence when considering expander real operating conditions, as expansion process is not strictly adiabatic [15].

Regarding the expansion machines used in micro-scale ORC systems, nowadays the available solutions are mostly volumetric architectures, in-house manufactured, usually derived from compressors designed for the HVAC&V sector [16]. Models of semi-empirical type can be the better choice for simulating positive displacement expanders, since they offer a good trade-off between simulation speed, calibration efforts, modelling accuracy and robust extrapolation capability [17]. In addition, they are demonstrated to be more precise in predict off-design performance rather than constant-efficiency and polynomial-based models [18] in micro-ORCs simulation. Some of those reported in the literature adopt an approach of lumped parameters type, dividing the expansion process into two or more transformations and accounting for several sources of losses [19], [20]. Others are based on empirical correlations that define efficiencies and working conditions of the machines, based on experimental trends [18]. In [21] a comparison of the effectiveness of two models of the abovementioned types have been presented, applied on the same piston

expander analyzed in this work, finding an overall better accuracy of the lumped parameters approach. The pump component is less investigated compared to the expander, although of fundamental importance. Indeed, pump irreversibilities can substantially decrease the cycle overall efficiency [5]. Semi-empirical models have been successfully applied to volumetric pumps too [22], with the objective of understanding and predicting the behavior when operating at different conditions. However, literature on pump performance evaluation when employing different working fluids is still missing, especially concerning new HFOs.

In the view of the above, literature suggests that further experimental and numerical analyses are necessary to assess performance of R134a low-GWP alternatives into ORC systems. In this paper, the Authors want to give a contribution to fill this knowledge-gap and to extend the literature data of the mentioned and promising HFOs. A comparative investigation of the performance of a reciprocating expander, working with low-GWP fluids as replacement of HFC-134a, is presented. The expander on which the analysis is conducted is the three-piston prototype [23] currently installed in a micro-ORC test bench at the University of Bologna (UNIBO-ORC test bench). The expander in exam can be considered a representative volumetric geometry indicated for future micro-ORC systems and in particular it is designed to work with R134a and fluids with similar properties, such as new olefins R1234yf and R1234ze(E) [23].

In previous work of the Authors the expander and the whole system have been tested with R134a over a wide range of operating conditions [24]; moreover, a semi-empirical model has been implemented, calibrated and validated versus the available experimental data, in order to simulate the prototypal machine at different operating conditions than the reference case [25]. The objective of this study is to use the validated model to simulate the expander performance in case of replacing R134a with its low-GWP alternative fluids, namely R1234yf and R1234ze(E). With this purpose, the original model (based on the work of Glavatskaya et al. [20]) has been modified with the procedure proposed by Giuffrida [15], implemented to generalize a semi-empirical model to be used with a fluid other than the one for which the model was developed in the first place. A simplified model of the feed pump is here introduced to be integrated with the expander one, with the aim of predicting the expander performance in its real operation into the actual cycle. As done for the expander model, a thermodynamically realistic procedure was applied to generalize the model to simulate fluids other than R134a. In addition, the integrated model here proposed allows to identify the optimal built-in volume ratio that maximizes the electric power output in design conditions. This result may be used to modify the valve timing in order to improve the performance of the expander under investigation.

The main novel contribution of this work can be summarized by the following points:

- An investigation on the performance of a piston expander in a kW-scale ORC system, working with low-GWP fluids as drop-in replacement to HFCs is conducted. Semi-empirical models are employed to consider actual operating conditions, differently from less realistic constant isentropic efficiency assumptions. The aim is to examine how the different thermodynamic characteristics of the fluids could influence the expander and pump performance
- A previously validated model of the expander has been coupled with a model of the pump, in order to realize an integrated model that reproduces the real operation of the expander into the micro-ORC system.
- Both the models have been generalized in order to account for the change of the working fluid; in particular, a procedure for correcting the pump model is introduced for the first time.
- Semi-empirical model of the expander also allows to account for the influence of geometrical aspects, such as the built-in volume ratio, over the expander performance. Thus, the proposed integrated model has been used to optimize the built-in volume ratio, modifying the intake stroke ratio, in order to achieve the best performance of the expander under investigation for all the analyzed working fluids. With this final step, the Authors intend to propose a quite simple methodology to: i) identify the optimal intake stroke ratio value; ii) highlight the importance of optimizing this parameter for the specific expander operating conditions; iii) explore the micro-ORC best achievable performance.

## 1. WORKING FLUIDS ANALYSIS

Several HFOs organic fluids are now commercially available, but just a few of them are suitable for low temperature heat recovery applications. In particular, HFO refrigerants considered in this study as substitute of R134a are R1234yf and R1234ze(E). The main properties of R1234yf and R1234ze(E) have been reported and compared with the ones of R134a in Table 1, in Figure 1 and Figure 2, which show respectively the

saturation curves of the fluids on the T-s diagram and the saturation pressure as function of temperature (all the thermodynamic properties have been calculated using the open source library CoolProp [7]).

The data highlight the similar thermodynamic properties of the new HFO fluids compared to R134a while exhibit a significantly lower GWP value. Nevertheless, some differences exist, influencing the performance of the ORC components, specifically if working with pump and expander of volumetric type.

One of the main factors of influence over the cycle performance is the expansion pressure ratio (β), that depends on the pressures at which the fluid evaporates and condenses into the cycle at given temperatures of the hot and cold source respectively. To provide just an indication, saturation pressures at 75 °C and at 20 °C for the three fluids are reported in Table 1: it can be noticed that those of R134a and R1234yf are very similar, while values for R1234ze(E) are slightly lower. Corresponding pressure ratio is lower for R1234yf ($\beta \approx 3.8$) than the other two ($\beta \approx 4.2$). Other factors that especially influence the performance of the volumetric machines, as will be demonstrated hereinafter, are the liquid density and the viscosity of the fluid: a higher value of the former (observed for R134a) determines, at given mass flow rate and pressure head, a lower pump consumption, while the viscosity mainly affects pump leakage and thus its volumetric performance.

**Table 1**. Main properties of the substitute fluids compared with R134a [7].

| **Properties** | **Fluids** | | |
|---|---|---|---|
| | **HFC - 134a** | **HFO - 1234yf** | **HFO - 1234ze(E)** |
| Critical temperature (°C) | 101.06 | 94.7 | 109.37 |
| Critical pressure (bar) | 40.59 | 33.82 | 36.36 |
| Molar mass (g/mol) | 102.03 | 114.04 | 114.04 |
| Saturation pressure at 20 °C (bar) | 5.72 | 5.92 | 4.27 |
| Saturation pressure at 75 °C (bar) | 23.64 | 22.72 | 18.00 |
| Latent heat of evaporation at 20 °C (kJ/kg) | 182.28 | 149.29 | 170.63 |
| Latent heat of evaporation at 75 °C (kJ/kg) | 115.9 | 88.02 | 117.33 |
| Saturation liquid density at 20 °C (kg/m$^3$) | 1225.33 | 1109.86 | 1179.28 |
| Saturation vapour density at 75 °C (kg/m$^3$) | 137.48 | 158.51 | 107.67 |
| Saturation liquid viscosity at 20 °C (Pa/s) x $10^4$ | 2.07 | 1.54 | 2.00 |
| Safety group | A1 | A2L | A2L |
| 100 years – Global warming potential | 1430 | 4 | 6 |
| Ozone depletion potential | 0 | 0 | 0 |

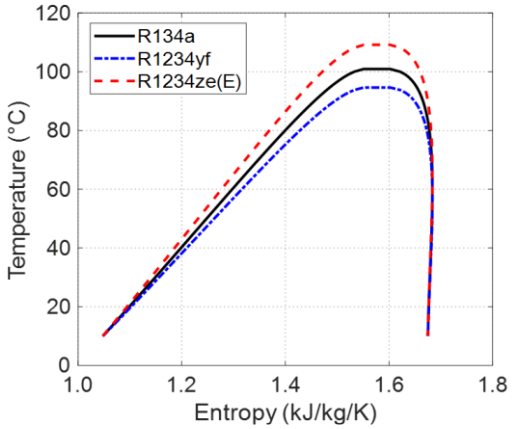


**Figure 1.** Saturation curves of the analyzed fluids on the Temperature-entropy diagram.

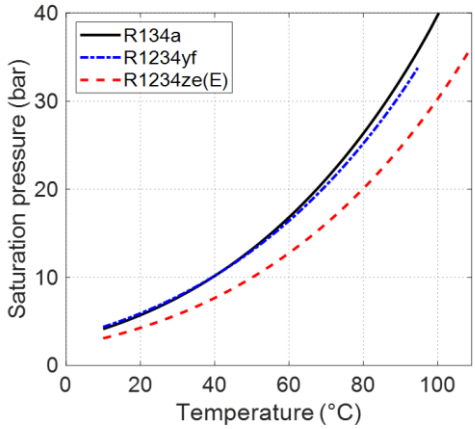


**Figure 2.** Saturation pressure of the analyzed fluids as function of the temperature.

## 2. THE EXPERIMENTAL SETUP

The ORC test bench used for the validation of the model is the one reported in Figure 3. The Authors presented in [24] a full characterization in steady state conditions, working with R134a. Briefly, it consists of a kW scale recuperated ORC, conceived for heat source temperature below 100 °C. The heat exchangers of the cycle are commercial brazed plate (evaporator and recuperator) and shell-and-tube (condenser) heat

exchangers. The key component of the system is the expander, a prototype of reciprocating model developed by the Italian company StarEngine [23]. It is made of three cylinders placed radially at 120° with a total displacement of 230 $cm^3$/rev. The admission and the discharge of the vapor at the expander are executed by rotatory valves, which are placed in correspondence of the cylinder head and are driven by the crankshaft rotation. The expander is directly coupled with the generator, which is connected to an electrical load, made of five pure resistive loads, connected in parallel between them and in delta with the generator output three-phase line. In this configuration, the load does not allow setting the generator rotational speed nor the load torque, and the expander shaft is free to achieve the equilibrium between the generator torque and the set load resistance. The feed pump is an external gear type and was also fabricated by StarEngine. It is driven by an asynchronous electric motor, to which is coupled through a speed reducer with gear ratio of 1:3. The pump motor is driven by a frequency inverter, which allows a proper regulation of the flow rate of the working fluid, since the pump is of positive displacement type. The thermal input to the ORC circuit is provided by a water loop heated by an electric boiler, whilst the cooling system consists in cold water extracted from a well.

The test bench is then fully equipped with an acquisition system, made of T-type thermocouples, ceramic pressure transducers and a Coriolis mass flow meter. Voltage and current transducers are installed on expander and pump supply lines for acquiring electrical power and frequency of the two machines.

In order to collect data in specific testing conditions, four main parameters (i.e. ORC boundary conditions) can be controlled from the outside: the water temperature at the evaporator inlet ($T_{H2OhotIN}$), the water temperature at the condenser inlet ($T_{H2OcoolingIN}$), the feed pump frequency ($f_{pump}$) and the number of activated resistive loads ($n_{loads}$). In Figure 3 a simplified layout of the test bench is reported. For further information, the reader can refer to [24], which presents a complete description of the test-rig, acquisition system and the extensive experimental campaign performed on the micro-ORC system.

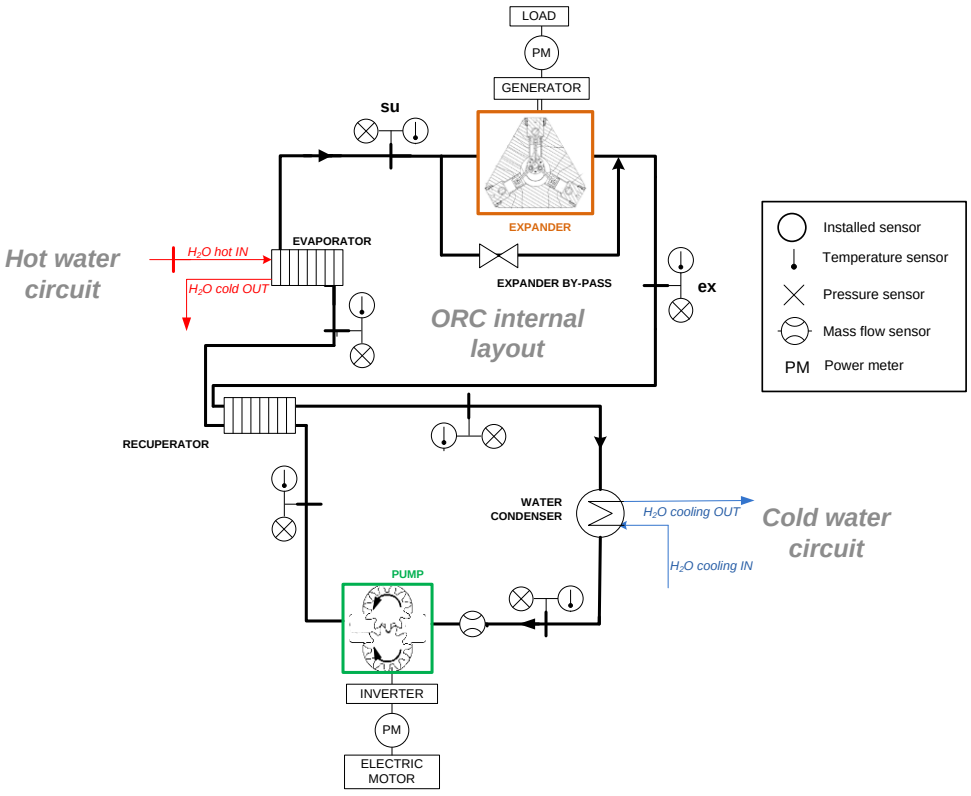


**Figure 3**. ORC test bench simplified layout.

## 3. MODEL DESCRIPTION

The model adopted is the integration of two semi-empirical models, describing the expander and pump behavior in steady-state conditions. The pump and the expander sub-models (detailed in the following paragraphs) have been integrated into a comprehensive calculation code, with the purpose of simulating the

expander behavior in its real operation into the cycle. The expander model was already introduced in [25], while the pump model has been introduced in this study in order to link the evaporation pressure and the organic fluid mass flow rate, which are in a strict correlation, as also demonstrated by the experimental trend of expander supply pressure ($p_{su}$) as function of the flow rate of R134a (see Figure 4). The choice of a semi-empirical approach, rather than constant-efficiency or polynomial-based model, assures a more realistic simulated performance especially in off-design conditions, with robust prediction in both fitting and extrapolation [18]. This kind of models rely on a set of physically meaningful equations whose parameters can be tuned to fit a reference dataset, or imposed where known. In this study, the data collected during the reference rig experimental tests [24] using R134a have been used for the calibration. Empirical parameters requiring calibration are described in detail in "Expander model" and "Pump model" subparagraphs. To account for the change of the working fluid, only the empirical parameters associated to the thermodynamic properties of the fluid must be corrected, while those related to the geometry of the components are kept equal to the reference case.

A schematic of the integrated model is shown in Figure 5; the inputs of the model are the boundary conditions of the system (water temperature at the condenser inlet, $T_{H2OhotIN}$, water temperature at the evaporator inlet $T_{H2OcoolingIN}$, feed pump frequency, $f_{pump}$, and number of resistive loads activated, $n_{loads}$): this choice allows to perform a fair comparison of the performance of the system when changing the working fluid, considering the same temperature of the hot and the cold sources, the same pump characteristic and the same system load. The condensation temperature determines the condensation pressure of the cycle ($p_{ex}$), assumed to be equal to the saturation pressure at the condensation temperature plus a temperature difference ($\Delta T$) at the condenser. The hot source temperature, instead, determines the expander inlet temperature ($T_{su}$), assumed to be equal to the hot source temperature minus a temperature difference ($\Delta T$) at the evaporator. The pump model requires as input the pump frequency ($f_{pump}$), the number of resistive loads ($n_{loads}$), and the condensation pressure ($p_{ex}$), to give, as output, the mass flow rate ($\dot{m}$) and the pump exhaust pressure ($p'_{su}$). The expander inlet pressure ($p_{su}$) is computed by subtracting to $p'_{su}$ the term $\Delta p_{loss}$, representing the pressure loss the fluid encounters between the pump outlet and the expander inlet (sum of recuperator and evaporator pressure losses). The organic fluid mass flow rate at the outlet of the pump is equal to the mass flow rate that enters into the expander, in steady-state conditions. The organic fluid mass flow rate and the evaporation pressure ($p_{su}$), together with the temperature at the inlet of the expander ($T_{su}$), and the condensation pressure ($p_{ex}$), are the inputs of the expander model. The outputs of the expander model coincide with the outputs of the integrated model and they are the shaft rotational speed of the expander ($N_{exp}$), the electric power output ($\dot{W}_{el}$) and the expander outlet temperature ($T_{ex}$).

The integrated model has been implemented in the Matlab environment [26] and the thermodynamic properties of the fluids have been calculated by means of the CoolProp library [7].

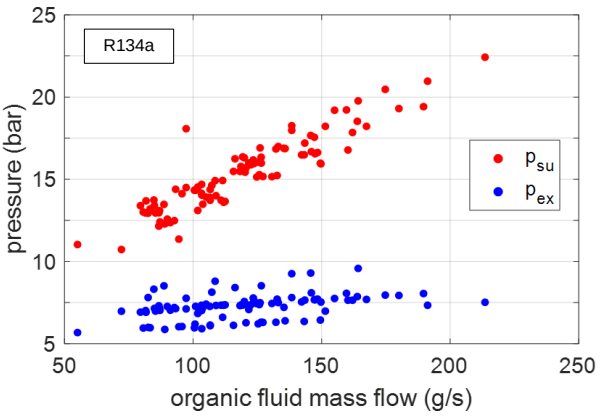


**Figure 4.** Experimental data of expander supply and exhaust pressure vs organic fluid mass flow.

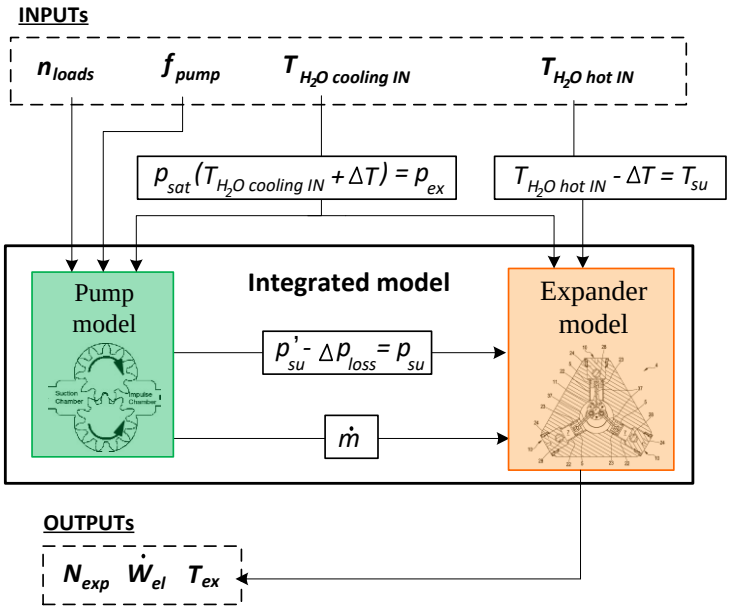


**Figure 5.** Schematic of the integrated model.

### 3.1 Expander model

The volumetric expander is simulated by means of the grey-box model originally developed by Glavatskaya et al. [20], adapted and validated for the reference reciprocating expander in a previous work of the Authors [25]. A summary of the input, output, constant values and calibrated model parameters (over R134a [25]) is provided in Table 2. The model follows a lumped parameters approach as illustrated in Figure 6. Equations of the model describe the internal expansion, the re-compression phenomena (based on the scheme and the p-V diagram shown in Figure 6) and additional characteristic power losses, such as under/over-expansion losses, pressure losses, internal leakages, heat dissipation, frictions and electro-mechanical conversion losses.

**Table 2.** Summary of the input, output, constant values and expander calibration parameters [25].

| **Inputs** | **Model parameters** | | **Calibrated value** | | **Outputs** |
|---|---|---|---|---|---|
| $T_{su}$ | $(AU)_{su,ref}$ | Supply heat transfer coefficient | 5.65e-05 | (W/K) | $T_{ex}$ |
| $p_{su}$ | $(AU)_{ex,ref}$ | Exhaust heat transfer coefficient | 9.23e-05 | (W/K) | $N_{exp}$ |
| $p_{ex}$ | $(AU)_{amb}$ | Ambient heat transfer coefficient | 0.96 | (W/K) | $\dot{W}_{el}$ |
| $\dot{m}$ | $r_{v,exp}$ | Built-in volume ratio | 1.459 | - | |
| | $r_{v,comp}$ | Re-compression volume ratio | 1.25 | - | |
| **Constants** | $V_0$ | Clearance volume | 2.32e-02 | ($cm^3$) | |
| Swept volume $Vs$ = 230 $cm^3$, | $A_{leak}$ | Equivalent leakage area | 5.51e-06 | ($m^2$) | |
| Electro-mechanical conversion efficiency = 90 % | $A_{su}$ | Supply nozzle equivalent section | 1.47e-05 | ($m^2$) | |
| | $W_{loss,ref}$ | Constant friction losses | 0.198 | (W) | |
| | $W_{loss,N}$ | Proportional friction losses | 1.07e-05 | (W/min) | |

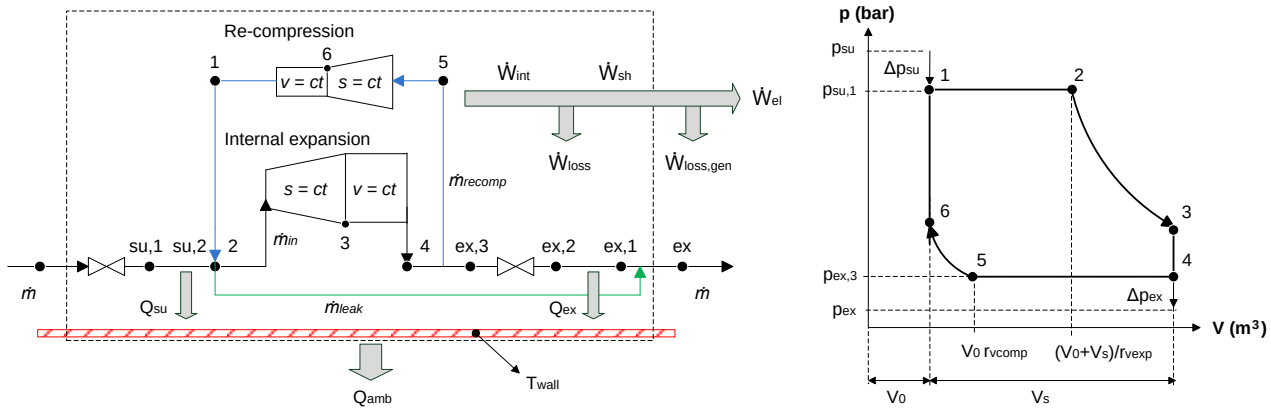


**Figure 6.** Scheme of the model and associated p-V diagram.

The main model physical equations are here briefly reported for lecturer convenience. Anyway, the lecturer is invited to refer to [25] for a detailed description. In particular, the electric power ($\dot{W}_{el}$) and the shaft rotational speed of the expander ($N_{exp}$), outputs of the expander model, are calculated by means of Eqs. (1-2). The electric power, $\dot{W}_{el}$, is expressed by the difference between the expansion power, and the power lost for re-compression and friction loss, as:

$$\dot{W}_{el} = \left[\dot{m}_{in} \cdot (h_2 - h_4) - \dot{m}_{recomp} \cdot (h_1 - h_5) - \dot{W}_{loss}\right] \cdot \eta_{conv} \quad (1)$$

Where $\eta_{conv}$ is the electro-mechanical conversion efficiency.

The rotational speed, $N_{exp}$, is obtained as:

$$N_{exp} = 60 \cdot \dot{m}_{in} / (\rho_2 \cdot V_2 - \rho_6 \cdot V_6) \quad (2)$$

The expansion and the recompression transformations are modelled using the volumetric expansion ratio, $r_{v,exp}$, and the volumetric compression ratio, $r_{v,comp}$ (see p-v diagram of Figure 6). The two volumetric ratios are used to compute the fluid state at the end of the expansion process, after an isentropic and a subsequent isochoric transformation.

The mass flow rate that undergoes the internal expansion is given by the difference between the flow rate entering the expander and the leakage flow. The leakage mass flow rate ($\dot{m}_{leak}$) is calculated, using equation Eq. (3), assuming an isentropic flow through a convergent nozzle, with a throat section area equal to the parameter $A_{leak}$, $\rho$ is the vapour density and $\Delta h$ is the enthalpy drop that occurs through the valve; the outlet enthalpy is evaluated with the throat critical pressure, assuming chocking conditions.

$$\dot{m}_{leak} = \rho \cdot A_{leak} \cdot \sqrt{2 \cdot \Delta h} \quad (3)$$

The mass flow rate that undergoes recompression, $\dot{m}_{recomp}$ , is calculated as function of the clearance volume, $V_0$, according to:

$$\dot{m}_{recomp} = \frac{V_0 \cdot \rho_4 \cdot N}{60} \quad (4)$$

Finally, the overall mechanical losses are accounted in $\dot{W}_{loss}$ term. This contribution is calculated in the model by accounting for two different terms: a constant term, $\dot{W}_{loss,ref}$ representing the constant mechanical loss and a second contribute, $\dot{W}_{loss,N}$ proportional to the rotational speed.

Other contributions of loss affecting also the output temperature ($T_{ex}$) are due to the pressure drop at the supply and exhaust valves and the heat dissipations. The supply pressure drop is modelled as an isentropic expansion through a convergent nozzle, using an equation similar to Eq. (3). The heat exchanged at the supply and exhaust section, $\dot{Q}_{su/ex}$, is obtained by means of the NTU method, according to the following three equations:

$$\dot{Q}_{su/ex} = \varepsilon \cdot c_p \cdot \dot{m} \cdot (T_{fluid} - T_{wall}) \quad (5)$$

$$\varepsilon = 1 - e^{-NTU} \quad (6)$$

$$NTU = \frac{1}{c_p \cdot \dot{m}} \cdot AU_{su/ex,ref} \cdot \left(\frac{\dot{m}}{\dot{m}_{ref}}\right)^{0.8} \quad (7)$$

where $\dot{m}_{ref}$ is the reference mass flow rate value, while $AU_{su/ex,ref}$ is the reference global heat transfer coefficient value. The heat exchanged with the ambient, $\dot{Q}_{amb}$, is computed as product between the ambient heat transfer coefficient $AU_{amb}$ and the temperature difference between the wall and the ambient; the wall temperature is calculated by the energy balance:

$$\dot{W}_{loss} + \dot{Q}_{ex} - \dot{Q}_{amb} + \dot{Q}_{su} = 0 \quad (8)$$

### 3.3 Correction of the heat transfer parameters of the expander model

The expander model has been here modified in order to predict the performance of the expander with different fluids than the one for which the model was calibrated. The model adaptation derives from the procedure proposed by Giuffrida [15] to express the heat transfer losses. The model parameters used to obtain the thermodynamic state of the fluid at the inlet and outlet side of the internal expansion process are adjusted. In particular, the key parameters to be corrected are the product of global heat transfer coefficient and heat exchange area in reference conditions of expander inlet and outlet, $(AU)_{su,ref}$ and $(AU)_{ex,ref}$ ; these parameters are used to model the heat transfer between the working fluid and the casing, as described by Eqs. (5-7).

The heat transfer coefficient, or thermal transmittance, *U*, is evaluated as:

$$U = \frac{Nu \cdot \lambda}{L} \quad (9)$$

where $Nu$ is the Nusselt number, $\lambda$ is the conductivity and $L$ is the characteristic length. The Nusselt number is calculated using the Dittus-Boelter correlation for turbulent flows:

$$Nu = 0.023 \cdot \mathrm{Re}^{0.8} \cdot \mathrm{Pr}^{a} \quad (10)$$

where *a* is equal to 0.4 if the fluid is heated by the wall, or it is equal to 0.3 if the fluid is cooled by the wall. Given that the characteristic length is set and the velocity do not depend on the working fluid (being set the flow passage area and the swept volume), the global heat transfer parameter for the new fluid, $(AU)_{ref,fluid}$, can be determined by manipulating equation (11).

$$\frac{(AU)_{ref,fluid}}{(AU)_{ref,R134a}} = \frac{Nu_{fluid} \cdot \lambda_{fluid}}{Nu_{R134a} \cdot \lambda_{R134a}} \quad (11)$$

$$(AU)_{ref,fluid} = (AU)_{ref,R134a} \cdot \left(\frac{\rho_{fluid}}{\rho_{R134a}}\right)^{0.8} \cdot \left(\frac{c_{pfluid}}{c_{pR134a}}\right)^{a} \cdot \left(\frac{\lambda_{fluid}}{\lambda_{R134a}}\right)^{1-a} \cdot \left(\frac{\mu_{R134a}}{\mu_{fluid}}\right)^{0.8-a} \quad (12)$$

where $\rho$ is the fluid density, $c_p$ is the heat capacity at constant pressure and $\mu$ the fluid viscosity; the subscript *fluid* indicates the quantities related to the new fluid, while the subscript *R134a* indicates those referred to R134a. Equation (12) is applied to both the parameters $(AU)_{su,ref}$ and $(AU)_{ex,ref}$. The thermodynamic properties of the fluids included into equation (12) have been evaluated in a reference operating point: the reference state for the parameter $(AU)_{su,ref}$ is defined by a pressure of 15 bar and a temperature of 75 °C, while the reference state for $(AU)_{ex,ref}$ is defined by a pressure of 7 bar and a temperature of 50 °C. The reference working point is selected as the most representative of the micro-ORC system operation; the corresponding supply and exhaust

pressure at the expander are the most frequently occurring and mean values during the experimental campaign (as confirmed by Figure 4).

The resulting corrected parameters are listed below in Table 3:

**Table 3:** Corrected heat transfer parameters for the expander model

| Parameters | Fluids | | |
|---|---|---|---|
| | R134a | R1234yf | R1234ze(E) |
| $(AU)_{su,ref}$ (W/K x $10^5$) | 5.65 | 6.38 | 6.53 |
| $(AU)_{ex,ref}$ (W/K x $10^5$) | 9.23 | 10.19 | 10.13 |

As regards the other model parameters listed in Table 2, $(AU)_{amb}$ is not dependent on the working fluid, since it describes just the heat losses from the casing to the ambient; thus, it does not require to be corrected when changing the fluid. Same goes for the parameters $r_{v,exp}$, $r_{v,comp}$, $V_0$, $A_{leak}$ and $A_{su}$, which are geometrical parameters, characteristic of the specific machine. Eventually, the values of the parameters $W_{loss,ref}$ and $W_{loss,N}$, which take into account the friction losses, are kept equal to the ones obtained for the R134a, according to [15]. Actually, a more detailed modelling approach could include both the Coulomb and the viscous friction terms in the friction losses formulation, which instead would depend on the fluid viscosity. Nevertheless, friction losses represent a limited contribution compared to the other loss sources (as demonstrated later in the results paragraph), thus, the modification of the model friction parameters can be neglected in the model applied in this study.

### 3.4 Pump model

When considering the expander model by itself, the evaporation pressure ($p_{su}$) and mass flow rate ($\dot{m}$) of the working fluid are two independent input variables of the model; on the contrary, if one wants to simulate the behavior of the machine when coupled to a pump in a real system, the two variables are related. Thus, in order to simulate the changing of the fluid in the real operation of the system, this relationship must be defined introducing a pump model that associates pump speed with outlet pressure.

Generally, pump models are described by means of performance maps reporting pressure head versus volumetric flow rate at different rotating speeds. The actual operating point of the pump is then determined by crossing the characteristic curve of the pump with the resistance characteristic of the system in which the pump is inserted. For the case study, the characteristic curve of the pump and the resistance characteristic of the system have been traced by interpolating the experimental data, collected by testing the system with R134a (see Figure 7 and Figure 8).

Data concerning the pump performance have been collected during the experimental campaign conducted over the micro-ORC system [24]. Additional tests have been performed with the expander by-passed, with the specific aim of completing the characteristic curves at low pressure head values, which cannot be reached when the expander is running. The procedure consisted in setting a pump frequency and adjusting a valve opening along the circuit to vary the flow rate and increase the circuit resistance. In this way, performance of the volumetric pump has been evaluated over a wider operating range, i.e. pressure rise going from 1 to about 10 bar and volume flow between 60 to 160 $cm^3/s$.

Figure 9 shows the extrapolated pump and circuit characteristic curves that constitute the operating map of the pump in exam. This operating map, once integrated into the model, allows to determine the actual pressure rise and the volume flow rate elaborated by the pump, for given conditions of pump frequency ($f_{pump}$) and number of activated resistive loads ($n_{loads}$) (i.e. the point of intersection of the actual pump line and the circuit resistance line). The mass flow rate, input of the expander model, is then obtained using the fluid density at the pump inlet, evaluated via CoolProp from condensing pressure and pump inlet temperature.

The actual resistance of the system is influenced by the number of the activated resistive loads dissipating the electric power generated by the expander. This is because the increase of the expander load determines a greater fluid dynamic resistance of the circuit, resulting in higher values of the pressure rise for given value of volume flow rate (obtainable with higher pump frequency, see Figure 9).

The observed pump volumetric performance is quite reduced at high pressure rise, according to the high slope of the pump characteristic curves of Figure 9, probably due to the gears wear out and/or to a non-correct amount of lubricant oil inside the circuit. For example, at rotational speed corresponding to pump frequency ($f_{pump}$) equal to 35 Hz and for a pressure rise equal to 8 bar, the actual volumetric flow is equal to 110 $cm^3/s$ while the theoretical volumetric flow is equal to 175 $cm^3/s$, corresponding to a volumetric efficiency equal to 63 %.

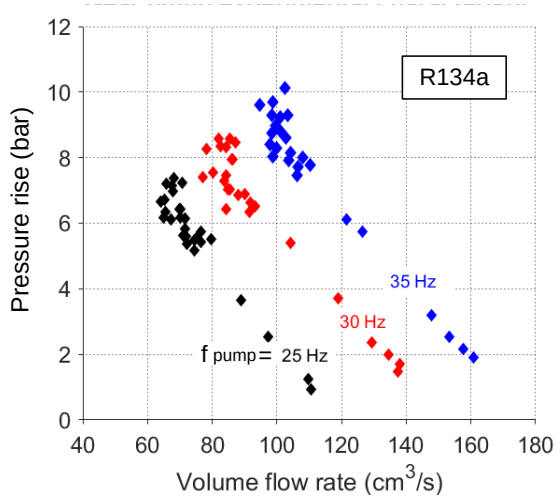


**Figure 7.** Experimental characteristic of the volumetric pump, working with R134a.

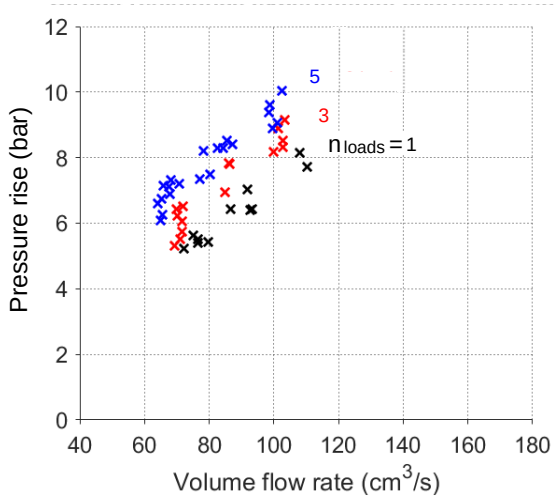


**Figure 8.** Experimental characteristic of the circuit resistance.

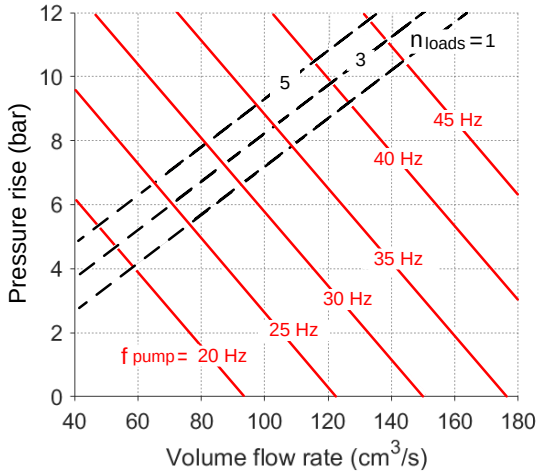


**Figure 9.** Extrapolated characteristic curves of the pump and resistance curves of the system.

### 3.5 Correction of the pump performance map

The characteristic curves of the pump have been adjusted in order to determine the new operating point of the pump when working with fluids different from R134a, according to the modelling approach described below.

To a first approximation, the volume flow rate actually elaborated by the pump, $\dot{V}$ , is equal to the difference between the theoretical volume flow rate that the pump could elaborate ($\dot{V}_{th}$) and the leakage flow rate lost through the meatus ($\dot{V}_{leak}$).

$$\dot{V} = \dot{V}_{th} - \dot{V}_{leak} \tag{13}$$

Due to the pressure rise, $\Delta p$, between inlet and outlet of the pump, a leakage occurs through its internal clearance, in particular, through the space between the tips of the gear teeth and the cavity wall. Poiseuilles law for laminar flow is here used to evaluate the leakage flow, $\dot{V}_{leak}$, through the meatus, as function of the viscosity of the fluid, $\mu$, of the meatus geometry and of the pressure rise between inlet and outlet, according to the following equation:

$$\dot{V}_{leak} = \frac{b \cdot h^3 \cdot \Delta p}{12 \cdot \mu \cdot l} \tag{14}$$

where $h$ is the meatus height, $l$ the length and $b$ the width. The theoretical volume flow rate is equal to the pump cubic capacity ($V_{cc}$) multiplied by the rotational speed ($N_{pump}$), which corresponds also to the value of the volume flow rate at null pressure rise.

$$\dot{V}_{th} = V_{cc} \cdot \frac{N_{pump}}{60} = \dot{V}(\Delta p = 0) \tag{15}$$

The set of equations (13–15) define the linear dependence of the pressure rise $\Delta p$ on the volume flow rate. Indeed, being constant the geometrical quantities, the expression of the pump pressure rise can be written as:

$$\Delta p = (c_1 \cdot N_{pump} - \dot{V} \cdot c_2) \cdot \mu \tag{16}$$

where $c_1$ and $c_2$ are constant, calculated as:

$$c_1 = \frac{c_2 \cdot V_{cc}}{60} \tag{17}$$

$$c_2 = \frac{12 \cdot \mathrm{l}}{\mathrm{b} \cdot h^3} \tag{18}$$

$c_1$ and $c_2$ are experimentally determined by interpolating the data collected during the test performed on R134a. The parameters values used in equation (16) are reported in Table 4.

Once the rotational speed is set, $\dot{V}$ is only affected by the fluid viscosity. Therefore, the effect of the change of the working fluid on the pump characteristic curve is a variation of the curve slope, as shown in Figure 10. Figure 10 compares the characteristic curves of the pump working with the different fluids at the same pump frequency equal to 30 Hz. For given values of rotational speed and pressure rise a fluid with lower viscosity provides lower volumetric flow rate values. The viscosity of the fluid has been evaluated, for all the analyzed fluids, in the reference condition of saturated liquid at 20 °C (see Table 1).

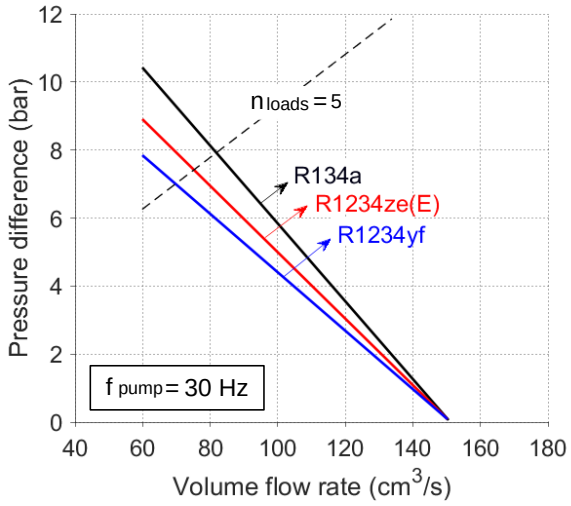


**Figure 10.** Characteristic curves of the pump, working with different fluids at the same pump frequency.

**Table 4.** Parameters values for the pump model.

| Parameter | Value |
|---|---|
| $c_1$ (-) | 5.65 x $10^2$ |
| $c_2$ ($cm^{-3}$) | 5.24 x $10^8$ |
| $V_{cc}$ ($cm^3$) | 64.7 |

## 4. RESULTS AND COMPARISON

The above described integrated model is used to simulate the behavior of the expander when changing the fluid. Two kinds of analysis have been performed: i) a first one investigates the change in the performance of the expander when varying the working fluid; ii) the second analysis aims at identifying the value of the volumetric expansion ratio that optimizes the electric power generation, for given design conditions.

### 4.1. Expander performance prediction with low-GWP fluids

A parametric analysis has been performed, for each analyzed fluid, setting the design conditions of hot source temperature, cooling source temperature and electric load, as indicated in Table 5; the feed pump frequency has been varied in the range 25 - 45 Hz. The corresponding Δp value has been obtained on the basis of the pump-circuit characteristic matching (see Figure 9). Figure 11 and Figure 12 relate respectively the pressure ratio and the superheating degree to the pump frequency. As expected, for a given fluid the pressure ratio increases with the pump frequency, since the evaporating pressure increases (see Figure 11), while the condensing pressure is constant, equal to the value imposed by the cold source temperature. Being constant the expander supply temperature, the superheating degree instead decreases versus the pump frequency (Figure 12). For a given pump frequency value, the use of R1234yf leads to lower pressure ratio and higher superheating degree values than in case of R134a, while the use of R1234ze(E) produces a higher pressure ratio and a lower superheating degree.

The results are shown in the form of performance maps curves of electric power output (Figure 13) and expander total efficiency (Figure 14). The expander total efficiency ($\eta_{exp}$) is calculated as the ratio between the electric power output ($\dot{W}_{el}$) and the isentropic power theoretically available for the expansion process ($\dot{W}_{is}$), i.e. the product between the mass flow rate ($\dot{m}$) and the isentropic enthalpy drop ($\Delta h_{is}$):

$$\eta_{exp} = \frac{\dot{W}_{el}}{\dot{W}_{is}} = \frac{\dot{W}_{el}}{\dot{m} \cdot \Delta h_{is}} \tag{19}$$

The results highlight that, for a given value of pressure ratio, the expander working with R134a achieves the highest value of electric power output, which decreases significantly when using R1234yf (- 24 %) and R1234ze(E) (- 44 %) in comparison with the R134a value. The expander total efficiency maximum value is obtained with R134a equal to 42 %, lower values of the maximum total efficiency are achieved respectively with R1234yf (37 %) and R1234ze(E) (35 %). It must be noticed that being different the evaporation pressure

and the condensation pressure values of the fluids considering the same value of the hot and cold source temperatures, the peaks of the total efficiency curves are not obtained at the same pressure ratio for the three analyzed fluids, as shown in Figure 14.

Two particular comparison cases between R134a and the new fluids, when feeding the same circuit, have been investigated: in one case the same pump frequency value (equal to 35 Hz) has been considered, in the second case the same superheating degree value (equal to 20 °C). In the latter case the pump speed is adjusted to reach a target value of superheating degree, which depends, at a given superheating temperature, on the evaporation pressure and thus on the flow rate of the organic fluid. Feed pump frequency and superheating degree values, for the fluids performance comparison, are chosen (respectively equal to 35 Hz and 20 °C) as the most representative of the regular operation of the micro-ORC system.

**Table 5**. Reference case condition for R134a performance simulation.

| | |
|---|---|
| **expander inlet temperature ($T_{su}$)** | 75 °C |
| **condensation temperature ($T_{H20\ cooling\ IN}$)** | 15 °C |
| **activated loads ($n_{loads}$)** | 5 |

| | |
|---|---|
| **feed pump frequency for comparison ($f_{pump}$)** | 35 Hz |
| **Superheating degree for comparison ($\Delta T_{sh}$)** | 20 °C |
| **Rotational speed for $r_{v,exp}$ optimization ($N_{exp}$)** | 832 rpm |

In Figure 13 and in Figure 14, operating points at the same pump frequency value are indicated by circular dots, whilst points at the same superheating degree are highlighted by square dots. The obtained results show that, for the pump frequency reference conditions of 35 Hz, the maximum electric power output is achieved with R134a, followed by R1234ze(E), for which the electric power output decreases of 23 % and by R1234yf with a decrease of 40 % (see circular markers in Figure 13). The performance derating of the expander when replacing R134a with low GWP fluids is also shown by the trends of the total efficiency in Figure 14. Indeed, the total efficiency achievable with R1234yf also decreases compared to R134a value, the same occurs for R1234ze(E). Even if R1234ze(E) allows to generate a higher value of electric power output compared to R1234yf, the latter achieves higher total efficiency value, in the reference conditions.

When comparing the fluids at the same superheating degree, the pressure ratio value becomes quite similar for all the fluids. The highest electric power output is achieved again with R134a, then by R1234yf, with a decrease in the electric power output of 28 % and then by R1234ze(E) with a reduction of 40 %. The same reduction in the expander performance is found in the total efficiency map (Figure 14).

The main factors that influence the expander performance are: (i) the saturation pressure (influencing the enthalpy drop available through the expander), (ii) the viscosity (mainly affecting the leakage losses at the pump meatus and thus the elaborated mass flow rate), (iii) the heat transfer coefficients values (influencing the ambient heat loss), (iv) the vapor density (affecting the leakage losses during the expansion process). The loss terms affecting the expander performance have been calculated by means of the proposed expander model, which accounts for valve pressure drop, internal leakage, under/ or over-expansion, heat transfer, friction and electro-mechanical conversion losses (for more details on the model equations, see [25]). The relative importance of the different losses affecting the expander performance, is represented in the pie charts of Figure 15, as percentage of the isentropic power theoretically available for the expansion process ($\dot{W}_{is}$).

The isentropic power values and other quantities of interest are reported in Table 6 for comparison. The fluids that exhibit higher isentropic enthalpy drop are R134a and R1234ze(E), with quite similar values. However, the fluid that presents the highest expansion isentropic power is R134a (2620 W), due to the highest mass flow rate at the expander inlet. Indeed, R134a is the fluid with the maximum liquid viscosity ($2.07 \times 10^{-4}$ Pa·s) and thus the minimum leakage loss at the pump meatus affecting volumetric flow (see Figure 9).

The heat losses are strongly related to the heat transfer coefficients, which are considered into the model by means of the heat transfer parameters (listed in Table 3). As expected, higher ambient heat loss results

from higher values of the heat transfer parameters, therefore the percentage heat loss of the low-GWP fluids is higher than that of R134a.

Both internal leakage and pressure drops across the valves depend on the density of the vapour entering the expander, as described in Eq. (3). Equation shows the inverse proportionality correlation between the pressure drop affecting $\Delta h$ over the valves and the vapour density. When evaluating the leakage mass flow rate, instead, equation shows the proportionality correlation between the internal leakage and the vapour density. On the basis of these correlations, fluids with higher vapour density (as HFOs, if compared to R134a, see Table 6) exhibit lower pressure drop losses, but also higher internal leakages, as shown by the pie charts of Figure 15.

The difference between the isentropic power and the sum of all the loss contributions finally corresponds to the electric power output value, indicated both in Figure 13 and in Figure 15. The percentage of generated electric power over the isentropic power is equal to the expander total efficiency value, shown both in Figure 14 and in Figure 15.

The comparative analysis, among R134a substitutes, at the same pump frequency identifies in the R1234ze(E) the best candidate to maximize the electric power output and minimize the environmental impact at the same time; conversely, comparison at the same superheating degree suggests R1234yf as a better choice. This is due to the different evaporation pressure assumed by the fluids, thus affecting the available amount of expansion isentropic power. Indeed, at the same pump frequency, R1234ze(E) presents higher pressure ratio and isentropic power, if compared to R1234yf. At the same superheating degree, the pressure ratio values are very similar, but the isentropic power is higher for R1234yf.

In conclusion, it must be highlighted that R134a presents higher performance than HFO fluids for all the examined conditions, thanks to both the higher isentropic power and the higher total efficiency values. However, whilst the electric power is remarkably higher for R134a compared to the other fluids, the total efficiency among the different fluids is not that different. This is because isentropic power available for most of the HFOs cases is lower than that available for R134a, as well as the total amount of lost power (see Table 6). Finally, it should be highlighted that the expander operates with reduced shaft speed ($N_{exp}$) values (see Table 6) in case of HFOs, in comparison with the reference R134a working condition.

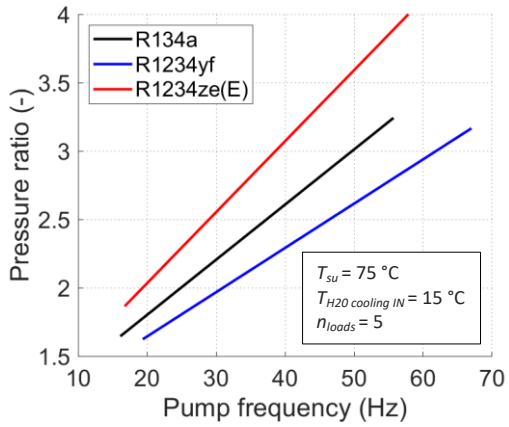


**Figure 11.** Trend of pressure ratio vs pump frequency: effect of the fluid variation.

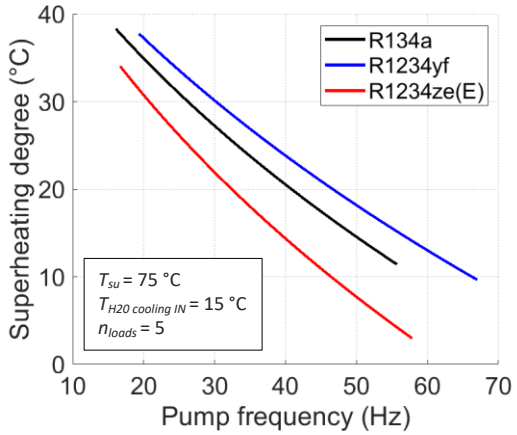


**Figure 12.** Trend of superheating degree vs pump frequency: effect of the fluid variation.

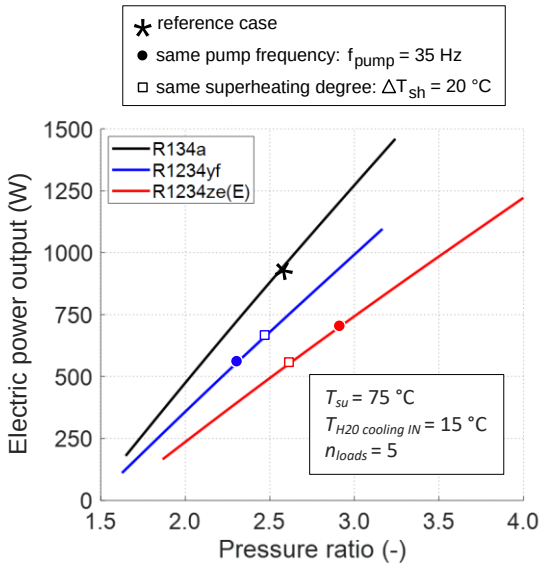


**Figure 13.** Electric power vs pressure ratio: effect of the fluid variation.

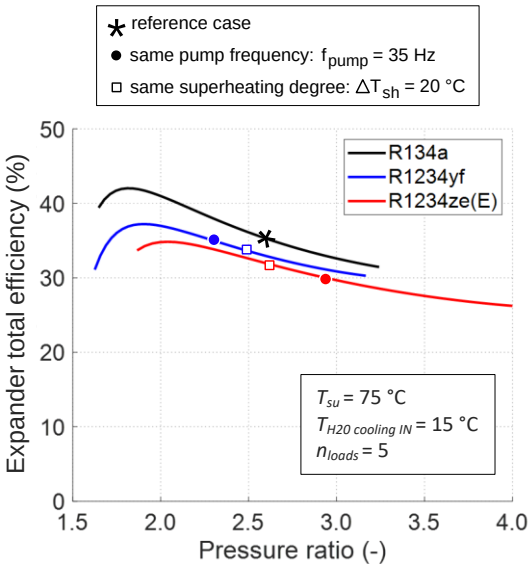


**Figure 14.** Trend of expander total efficiency vs pressure ratio: effect of the fluid variation.

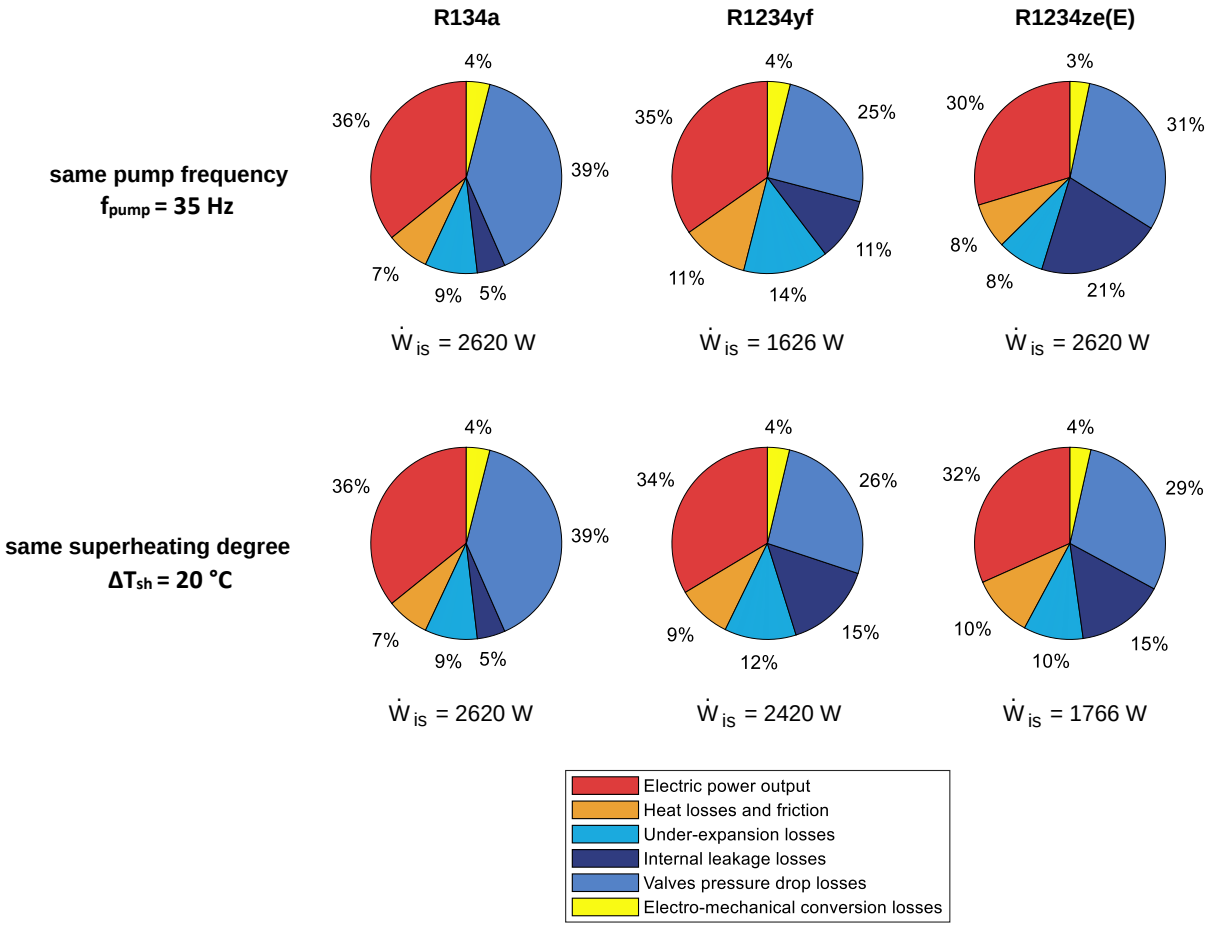


**Figure 15.** Analysis of loss contributions affecting the expander performance for the three working fluids. Values are expressed as percentage of the isentropic power theoretically available for the expansion process ($\dot{W}_{is}$).

**Table 6.** Fluids comparison. Percentual variation compared to the reference case are shown in parenthesis.

| | Reference case | Same pump frequency comparison | | Same superheating degree comparison | |
|---|---|---|---|---|---|
| | **R134A** | **R1234yf** | **R1234ze(E)** | **R1234yf** | **R1234ze(E)** |
| **Pump frequency, $f_{pump}$ (Hz)** | 35 | 35 | 35 | 40 | 30 |
| **Superheating degree, $\Delta T_{sh}$ (°C)** | 20 | 23 | 15 | 20 | 20 |
| **Evaporation pressure, $p_{su}$ (bar)** | 14.4 | 13.6 | 12.6 | 14.6 | 11.2 |
| **Condensation pressure, $p_{ex}$ (bar)** | 5.7 | 5.9 | 4.3 | 5.9 | 4.3 |
| **Isentropic enthalpy drop, $\Delta h_{is}$ (kJ/kg)** | 21.3 | 17.3 (-19 %) | 22.2 (+4 %) | 18.4 (-14 %) | 20.3 (-5 %) |
| **Mass flow rate, $\dot{m}$ (kg/s)** | 0.123 | 0.094 (-24 %) | 0.109 (-11 %) | 0.109 (-11 %) | 0.087 (-29 %) |
| **Vapor density (kg/m$^3$)** | 62.6 | 66.9 | 62.0 | 73.5 | 53.3 |
| **Expansion isentropic power, $\dot{W}_{is}$ (W)** | 2620 | 1626 (-38 %) | 2420 (-8 %) | 2006 (-23 %) | 1766 (-33 %) |
| **Heat transfer and friction (W)** | 183 | 179 | 194 | 181 | 177 |
| **Other losses (W)** | 1494 | 878 | 1500 | 1143 | 1024 |
| **Total losses (W)** | 1677 | 1057 | 1694 | 1324 | 1201 |
| **Electric power output, $\dot{W}_{el}$ (W)** | 943 | 569 (-40 %) | 726 (-23 %) | 682 (-28 %) | 565 (-40 %) |
| **Expander total efficiency, $\eta_{exp}$ (%)** | 36 | 35 | 30 | 34 | 32 |
| **Exhaust expander temperature, $T_{ex}$ (°C)** | 39.5 | 47.1 | 39.2 | 44.4 | 43.8 |
| **Shaft speed, $N_{exp}$ (rpm)** | 832 | 478 | 750 | 534 | 627 |

### 4.2. Built-in volume ratio optimization

The built-in volume ratio parameter ($r_{v,exp}$) corresponds to the volumetric expansion ratio of the machine, and it is defined as the ratio between the inlet volume at the end of the expansion ($V_3$) and the volume at the end of the admission stroke ($V_2$). For the case study, $r_{v,exp}$ has been optimized for each analyzed fluid, at given reference conditions corresponding to the reference operating point (as indicated in Table 5).

The trend of the specific work, the elaborated mass flow rate (Figure 16) and the electric power output (Figure 17), are plotted against the intake stroke ratio, for a value of the expander shaft speed equal to 832 rpm. The intake stroke ratio, named α, represents the piston relative swept volume at the moment when the intake valve closes, defined as:

$$\alpha = \frac{V_2 - V_1}{V_s} \tag{20}$$

Thus, α can be expressed as a function of $r_{v,exp}$ according to:

$$\alpha = \frac{1}{r_{v,exp}} \cdot \frac{1 - r_{v,exp} \cdot \gamma}{1 - \gamma} \tag{21}$$

where $\gamma$ is a geometrical parameter:

$$\gamma = \frac{V_1}{V_1 + V_s} \tag{22}$$

Since the stroke displacement of the expander in study is equal to $V_s$ = 230 cm$^3$ and the clearance volume is equal to $V_1 = V_0 = 2.32 \cdot 10^{-2}$ cm$^3$ (see Table 2), the intake stroke ratio $\alpha$ can be approximated as the inverse of the built-in volume ratio:

$$\alpha = \frac{1}{r_{v,exp}} \tag{23}$$

The bell curve of the electric power results by the combination of the opposite trends of the specific work and the elaborated mass flow rate, since the electric power output ($\dot{W}_{el}$) is proportional to the product of the two quantities. The specific work decreases when α increases, because of the under-expansion losses; conversely, the elaborated mass flow rate increases with α, because for a longer intake stroke more fluid has time to enters into the cylinder. In this case study, the maximum value of the electric power output is observed for $\alpha$ around 0.37, corresponding to a built-in volume ratio, $r_{v,exp}$ equal to 2.7, very close for all the three considered fluids. On the other hand, the current value of $\alpha$ is close to 0.69, corresponding to a value of $r_{v,exp}$ of 1.46. Figure 17 shows that the optimization of the built-in volume ratio for the case study could increase significantly the electric power output by 41 % for R134a and by 43 % for R1234yf and R1234ze(E), if compared to the producible electric power of the current configuration. A comparison between the indicator diagrams obtained with the optimal $\alpha$ value and the one obtained with the reference $\alpha$ value are reported in Figure 18, which highlights that reducing the intake stroke significantly decreases the under-expansion losses. Actually, a certain degree of over-expansion is preferred in order to ensure the exploitation of all the available pressure head.

Finally, in Table 7 the main performance results of the optimization of the built-in volume ratio are compared with those related to reference value of $r_{v,exp}$. The percentual increment of the expander efficiency is expected to be higher than the electric power one: indeed, the isentropic power, denominator of the efficiency expression, decreases due to the reduction of the mass flow rate, while the isentropic specific work remains the same, being the inlet and exhaust pressures equal to the reference case. Results of the simulation show potential remarkable efficiency gain of approximately 40 percentage points with respect to the case of $r_{v,exp}$ not optimized, similar for the three fluids. The maximum value is achieved in this case with R1234yf, around 83%. Even if an increase in the expander efficiency is expected, the values of total efficiency, obtained by the $\alpha$ optimization are purely theoretical. Such high values of the expander efficiency are indications that some simplifications are introduced in the expander model. First of all, the supply valve real opening behavior has been modelled in a simplified way: the expander model assumes the instantaneous opening and closing of the valves. Real valve behavior would probably cause a loss of actual mass flow rate elaborated by the expander; indeed, as demonstrated by [27] the valve characteristics play an unneglectable role on the reciprocating machine operation. Nevertheless, the procedure proposed is intended to demonstrate the importance of the optimization of the filling performance of the expander, in order to achieve the best overall performance of the machine. For this purpose, a modification of the valve timing would be required [27][28] in order to optimally exploit the external heat sources, regardless of the working fluid adopted.

This result has been shown in detail for the expander in study, but the same approach should be applied to different volumetric expander design and with different geometrical sizes; when the machine is called to operate in a micro-ORC application with the same fluids under investigation, a check and update of the built-in volume ratio is required.

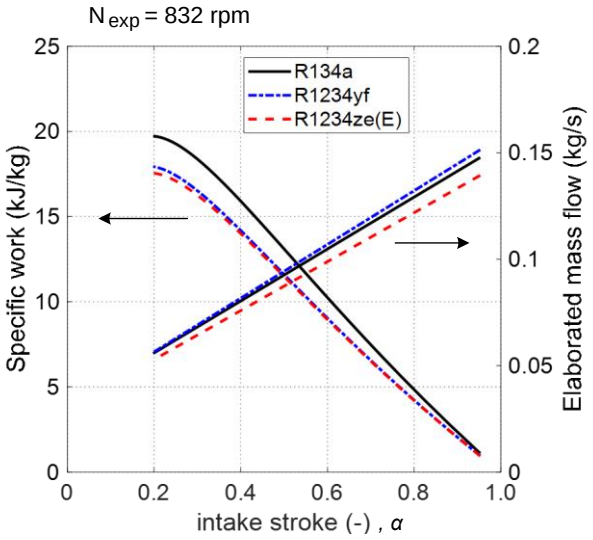


**Figure 16.** Trend of specific work and mass flow rate elaborated by the expander vs pressure ratio.

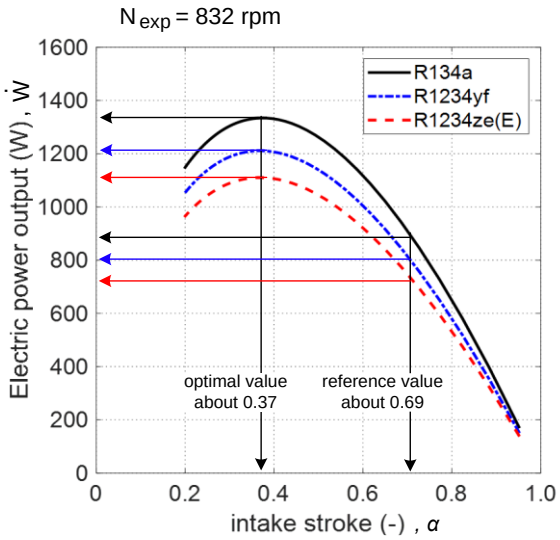


**Figure 17.** Trend of electric power output vs pressure ratio.

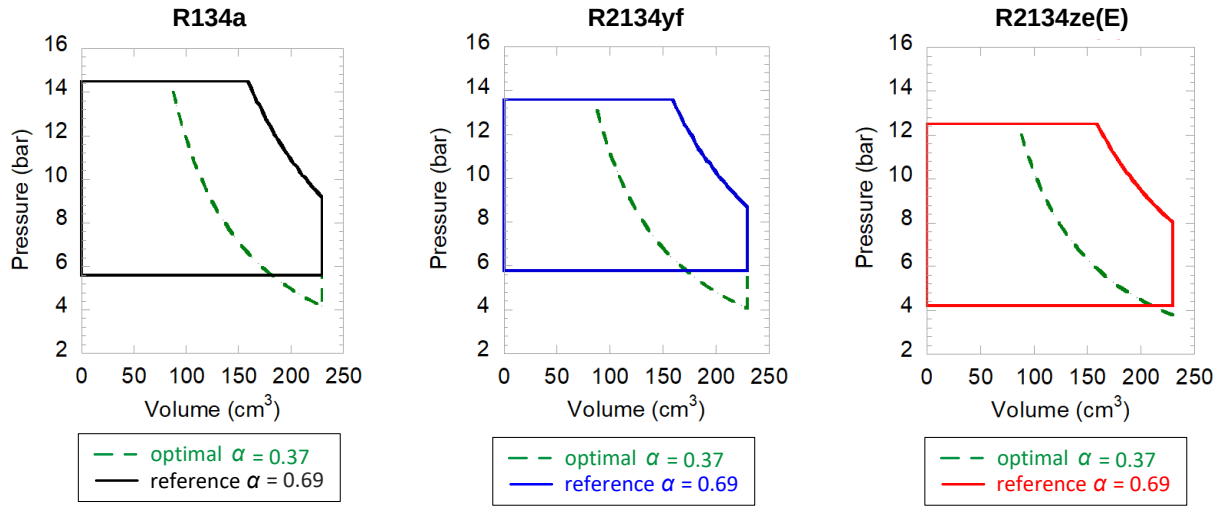


**Figure 18.** A comparison between the indicator diagrams obtained with the optimal $\alpha$ value and the one obtained with the reference $\alpha$ value.

**Table 7**. Main results of the built-in volume ratio optimization and comparison with reference case

| | R134a | | R1234yf | | R1234ze(E) | |
|---|---|---|---|---|---|---|
| | **Reference α = 0.69** | **Optimal α = 0.37** | **Reference α = 0.69** | **Optimal α = 0.37** | **Reference α = 0.69** | **Optimal α = 0.37** |
| Mass flow, $\dot{m}$ (kg/s) | 0.123 | 0.082 | 0.126 | 0.084 | 0.116 | 0.078 |
| Isentropic power $\dot{W}_{is}$ (W) | 2621 | 1747 | 2177 | 1452 | 2091 | 1406 |
| Electric power, $\dot{W}_{el}$ (W) | 943 | 1334 | 846 | 1211 | 775 | 1111 |
| Expander total efficiency (%) | 36 | 76 | 39 | 83 | 37 | 79 |

## 5. CONCLUSION

The purpose of this work was to investigate how the performance of a volumetric expander, working in a low temperature micro-ORC system, would change when using low GWP fluids (R1234yf and R1234ze(E)) to replace R134a as working fluid. To this purpose, the analysis was conducted on the reference case study of

a the three-piston prototype currently installed in a micro-ORC test bench at the University of Bologna (UNIBO-ORC test bench). The expander in exam is designed to work with R134a and fluids with similar properties, such as new hydrofluoroolefins R1234yf and R1234ze(E). Reliable experimental data related to the use of R134a as working fluid are available, as well as a validated model of the volumetric machine.

Semi-empirical models of the pump and the expander are employed in order to: i) consider actual operating conditions of the components when coupled in a real ORC circuit; ii) analyze in detail how the different thermodynamic characteristics of the fluids could influence the performance at component level. To this aim, both pump and expander models have been generalized in order to account for the change of the working fluid. The main modification regards the heat transfer parameters, which determines the heat transferred between the fluid and the expander wall. A procedure for correcting the pump model is also introduced, based on the correction of the slope of the characteristic curve according to the variation of fluid viscosity, which affects in particular fluid leakage through pump meatus (important aspect when using machines of volumetric type). Finally, the pump and the expander model have been integrated to reproduce expander real operation into the actual ORC cycle. The integrated model has been applied to compare the three fluids, considering the same temperature levels of the heat source and cold sink as well as the load connected to the expander generator, while for the feed pump rotating speed different cases have been examined (constant rotating speed, constant superheating degree).

First analysis highlight that, for a given value of pressure ratio, the expander working with R134a achieves the highest value of electric power output, which decreases significantly when using R1234yf (- 24 %) and R1234ze(E) (- 44 %). The same goes for the expander total efficiency, whose maximum value is obtained with R134a (42 %), followed by R1234yf (37 %) and R1234ze(E) (35 %), achieved at different values of the pressure ratio. However, two comparison cases between R134a and the new fluids, when feeding the same circuit, have been investigated: the first case considers the same pump frequency, while the second case considers the same superheating degree value. The comparative analysis, at the same pump frequency, identifies in the R1234ze(E) the best candidate to maximize the electric power output and minimize the environmental impact at the same time; conversely, comparison at the same superheating degree suggests R1234yf as better choice. However, R134a proves to be the most performing fluid among the analyzed ones, for all the examined case. Results of the analysis highlight that the performance of a volumetric expander into an ORC circuit actually depends on the pump regulation strategy and the fluid substitution decision should take into account also this aspect. In addition, even if the analysis is applied to a reference case study, findings related on how the fluid properties could affect expander and pump performance are generalizable. In particular, this study highlights that the main factors that affect the expander performance, when substituting R134a with its low-GWP alternatives, are: (i) the saturation pressure (influencing the enthalpy drop available through the expander), (ii) the viscosity (mainly affecting the leakage losses at the pump meatus and thus the elaborated mass flow rate), (iii) the heat transfer coefficients values (influencing the ambient heat loss), (iv) the vapor density (affecting the leakage losses during the expansion process). Relative importance of the different losses affecting the expander performance, is discussed in this paper.

The proposed integrated model has been used to optimize the built-in volume ratio, modifying the intake stroke ratio, in order to achieve the best performance of the expander under investigation for all the analyzed working fluids. With this final step, the Authors intend to propose a quite simple methodology to identify the optimal intake stroke ratio value; the same procedure is indeed applicable to different displacement expanders for optimizing the volumetric performance, depending on the specific working conditions the machine is required to work with. Results highlight that the optimization of the built-in volume ratio could lead to a substantial increase of the expander performance, with an estimated gain of electric power output around 42 %, similar for the three fluids. Thus, a modification of the valve timing would be required in order to optimally exploit the reference external heat sources, regardless of the working fluid adopted.

## REFERENCES

[1] Varma GVP, Srinivas T. Power generation from low temperature heat recovery. Renewable and Sustainable Energy Reviews 2017;75:402–14. https://doi.org/10.1016/j.rser.2016.11.005.
[2] Pereira JS, Ribeiro JB, Mendes R, Vaz GC, André JC. ORC based micro-cogeneration systems for residential application – A state of the art review and current challenges. Renewable and Sustainable Energy Reviews 2018;92:728–43. https://doi.org/10.1016/j.rser.2018.04.039.
[3] Tocci L, Pal T, Pesmazoglou I, Franchetti B. Small Scale Organic Rankine Cycle (ORC): A Techno-Economic Review. Energies 2017;10:413. https://doi.org/10.3390/en10040413.
[4] Park B-S, Usman M, Imran M, Pesyridis A. Review of Organic Rankine Cycle experimental data trends. Energy Conversion and Management 2018;173:679–91. https://doi.org/10.1016/j.enconman.2018.07.097.
[5] Quoilin S, Broek MVD, Declaye S, Dewallef P, Lemort V. Techno-economic survey of Organic Rankine Cycle (ORC) systems. Renewable and Sustainable Energy Reviews 2013;22:168–86. https://doi.org/10.1016/j.rser.2013.01.028.
[6] Regulation (EU) No 517/2014 of the European Parliament and of the Council of 16 April 2014 on fluorinated greenhouse gases and repealing Regulation (EC) No 842/2006 n.d.:36.
[7] Bell IH, Wronski J, Quoilin S, Lemort V. Pure and Pseudo-pure Fluid Thermophysical Property Evaluation and the Open-Source Thermophysical Property Library CoolProp. Ind Eng Chem Res 2014;53:2498–508. https://doi.org/10.1021/ie4033999.
[8] Heredia-Aricapa Y, Belman-Flores JM, Mota-Babiloni A, Serrano-Arellano J, García-Pabón JJ. Overview of low GWP mixtures for the replacement of HFC refrigerants: R134a, R404A and R410A. International Journal of Refrigeration 2020;111:113–23. https://doi.org/10.1016/j.ijrefrig.2019.11.012.
[9] Eyerer S, Dawo F, Kaindl J, Wieland C, Spliethoff H. Experimental investigation of modern ORC working fluids R1224yd(Z) and R1233zd(E) as replacements for R245fa. Applied Energy 2019;240:946–63. https://doi.org/10.1016/j.apenergy.2019.02.086.
[10] Yang J, Ye Z, Yu B, Ouyang H, Chen J. Simultaneous experimental comparison of low-GWP refrigerants as drop-in replacements to R245fa for Organic Rankine cycle application: R1234ze(Z), R1233zd(E), and R1336mzz(E). Energy 2019;173:721–31. https://doi.org/10.1016/j.energy.2019.02.054.
[11] Molés F, Navarro-Esbrí J, Peris B, Mota-Babiloni A, Mateu-Royo C. R1234yf and R1234ze as alternatives to R134a in Organic Rankine Cycles for low temperature heat sources. Energy Procedia 2017;142:1192–8. https://doi.org/10.1016/j.egypro.2017.12.380.
[12] Yamada N, Mohamad MNA, Kien TT. Study on thermal efficiency of low- to medium-temperature organic Rankine cycles using HFO−1234yf. Renewable Energy 2012;41:368–75. https://doi.org/10.1016/j.renene.2011.11.028.
[13] Le VL, Feidt M, Kheiri A, Pelloux-Prayer S. Performance optimization of low-temperature power generation by supercritical ORCs (organic Rankine cycles) using low GWP (global warming potential) working fluids. Energy 2014;67:513–26. https://doi.org/10.1016/j.energy.2013.12.027.
[14] Ancona MA, Bianchi M, Branchini L, De Pascale A, Melino F, Ottaviano S, et al. Performance prediction and design optimization of a kW-size reciprocating piston expander working with low-GWP fluids, Athens, Greece: 2019.
[15] Giuffrida A. Modelling the performance of a scroll expander for small organic Rankine cycles when changing the working fluid. Applied Thermal Engineering 2014;70:1040–9. https://doi.org/10.1016/j.applthermaleng.2014.06.004.
[16] Zhao Y, Liu G, Li L, Yang Q, Tang B, Liu Y. Expansion devices for organic Rankine cycle (ORC) using in low temperature heat recovery: A review. Energy Conversion and Management 2019;199:111944. https://doi.org/10.1016/j.enconman.2019.111944.
[17] Dumont O, Dickes R, Lemort V. Extrapolability and limitations of a semi-empirical model for the simulation of volumetric expanders. Energy Procedia 2017;129:315–22. https://doi.org/10.1016/j.egypro.2017.09.198.
[18] Dickes R, Dumont O, Daccord R, Quoilin S, Lemort V. Modelling of organic Rankine cycle power systems in off-design conditions: An experimentally-validated comparative study. Energy 2017;123:710–27. https://doi.org/10.1016/j.energy.2017.01.130.
[19] Lemort V, Quoilin S, Cuevas C, Lebrun J. Testing and modeling a scroll expander integrated into an Organic Rankine Cycle. Applied Thermal Engineering 2009;29:3094–102. https://doi.org/10.1016/j.applthermaleng.2009.04.013.

[20] Glavatskaya Y, Podevin P, Lemort V, Shonda O, Descombes G. Reciprocating Expander for an Exhaust Heat Recovery Rankine Cycle for a Passenger Car Application. Energies 2012;5:1751–65. https://doi.org/10.3390/en5061751.
[21] Bianchi M, Branchini L, De Pascale A, Melino F, Ottaviano S, Peretto A, et al. Performance prediction of a reciprocating piston expander with semi-empirical models. Energy Procedia 2019;158:1737–43. https://doi.org/10.1016/j.egypro.2019.01.403.
[22] D'Amico F, Pallis P, Leontaritis AD, Karellas S, Kakalis NM, Rech S, et al. Semi-empirical model of a multi-diaphragm pump in an Organic Rankine Cycle (ORC) experimental unit. Energy 2018;143:1056–71. https://doi.org/10.1016/j.energy.2017.10.127.
[23] Zampieri G. "Closed-cycle plant" U.S. Patent US2016/0032786A1, Feb. 4, 2016. US20160032786A1, 2016.
[24] Bianchi M, Branchini L, Casari N, De Pascale A, Melino F, Ottaviano S, et al. Experimental analysis of a micro-ORC driven by piston expander for low-grade heat recovery. Applied Thermal Engineering 2019;148:1278–91. https://doi.org/10.1016/j.applthermaleng.2018.12.019.
[25] Bianchi M, Branchini L, De Pascale A, Melino F, Ottaviano S, Peretto A, et al. Application and comparison of semi-empirical models for performance prediction of a kW-size reciprocating piston expander. Applied Energy 2019;249:143–56. https://doi.org/10.1016/j.apenergy.2019.04.070.
[26] MATLAB 2019b. Natick, Massachusetts, United States: © 1994-2020 The MathWorks, Inc.; n.d.
[27] Wronski J, Imran M, Skovrup MJ, Haglind F. Experimental and numerical analysis of a reciprocating piston expander with variable valve timing for small-scale organic Rankine cycle power systems. Applied Energy 2019;247:403–16. https://doi.org/10.1016/j.apenergy.2019.04.028.
[28] Antonelli M, Baccioli A, Francesconi M, Martorano L. Experimental and Numerical Analysis of the Valve Timing Effects on the Performances of a Small Volumetric Rotary Expansion Device. Energy Procedia 2014;45:1077–86. https://doi.org/10.1016/j.egypro.2014.01.113.

## NOMENCLATURE

**Symbols**

| | |
|---|---|
| $AU$ | Overall heat transfer coefficient (W/K) |
| $b$ | Meatus thickness (m) |
| $c_p$ | Specific heat at constant pressure (J/kg/K) |
| $ct$ | constant |
| $f$ | Frequency (Hz) |
| $h$ | Meatus height (m) |
| $h$ | enthalpy (J/kg) |
| $\dot{m}$ | Mass flow rate (kg/s) |
| $l$ | Meatus width (m) |
| $L$ | Characteristic length (m) |
| $N$ | Rotational speed (rpm) |
| $n$ | Number (-) |
| $Nu$ | Nusselt number (-) |
| $p$ | Pressure (Pa) |
| $Pr$ | Prandlt number(-) |
| $\dot{Q}$ | Heat flow (W) |
| $Re$ | Reynolds number (-) |
| $r_v$ | Volumetric ratio (-) |
| $T$ | Temperature (°C) |
| $s$ | Entropy (kJ/kg/K) |
| $U$ | Global heat transfer coefficient (W/m$^2$/K) |
| $V$ | Volume (m$^3$) |
| $\dot{V}$ | Volume flow rate (m$^3$/s) |
| $\dot{W}$ | Power (W) |

**Greek letters**

| | |
|---|---|
| $\alpha$ | Intake stroke ratio (-) |
| $\beta$ | Expansion ratio (-) |
| $\lambda$ | Conductive heat transfer coefficient (W·m/K) |
| $\Delta$ | Difference (-) |
| $\rho$ | Density (kg/m$^3$) |
| $\mu$ | Viscosity (Pa·s) |

**Acronyms**

| | |
|---|---|
| *COP* | Coefficient Of Performance |
| *CHP* | Combined Heat and Power |
| *GWP* | Global warming potential |
| *HFC* | Hydrofluorocarbons |
| *HFO* | Hydrofluoroolefines |
| *HVAC* | Heating Ventilation and Air Conditioning |
| *ORC* | Organic Rankine Cycle |

**Subscripts**

| | |
|---|---|
| *amb* | Ambient |
| *cc* | Cubic capacity |
| *el* | Electric |
| *ex* | Exhaust |
| *exp* | Expander |
| *fluid* | Fluid |
| *gen* | Generator |
| *H2O hot in* | Water at the evaporator inlet |
| *H2O cooling in* | Water at the condenser inlet |
| *int* | Internal |
| *is* | Isentropic |
| *leak* | Leakage |
| *loads* | Loads |
| *loss* | Loss |
| *pump* | Pump |
| *recomp* | Re-compression |
| *ref* | Reference |
| *R134a* | R134a |
| *sh* | Shaft |
| *su* | Supply |
| *s* | Swept |
| *th* | Theoretical |
| *wall* | Wall |
| *0* | Clearance |